Acta Oceanol. Sin., 2023, Vol. 42, No. 2, P. 65–73
https://doi.org/10.1007/s13131-022-2025-1
http://www.aosocean.com
E-mail: ocean2@hyxb.org.cn

Preliminary results of the global ocean tide derived from HY-2A radar altimeter data

Jungang Yang[1], Yongjun Jia[2]*, Chenqing Fan[1], Wei Cui[1]

[1] Lab of Marine Physics and Remote Sensing, First Institute of Oceanography, Ministry of Natural Resources, Qingdao 266061, China

[2] National Satellite Ocean Application Service, Beijing 100081, China

Received 24 August 2021; accepted 12 April 2022

Abstract

The HY-2A satellite, which is equipped with a radar altimeter and was launched on August 16, 2011, is the first Chinese marine dynamic environmental monitoring satellite. Extracting ocean tides is one of the important applications of the radar altimeter data. The radar altimeter data of the HY-2A satellite from November 1, 2011 to August 16, 2014 are used herein to extract global ocean tides. The constants representing the tidal constituents are extracted by HY-2A RA data with harmonic analysis based on the least squares method. Considering tide aliasing issues, the analysis of the alias periods and alias synodic periods of different tidal constituents shows that only the tidal constituents M_2, N_2, and K_2 are retrieved precisely by the HY-2A RA data. The derived tidal constants of the tidal constituents M_2, N_2 and K_2 are compared to those of tidal gauge data and the TPXO tide model results. The comparison between the derived results and the tidal gauge data shows that the RMSEs of the tidal amplitude and phase lag are 9.6 cm and 13.34°, 2.4 cm and 10.47°, and 8.1 cm and 14.19° for tidal constituents M_2, N_2, and K_2, respectively. The comparisons of the semidiurnal tides with the TPXO model results show that tidal constituents have good consistency with the TPXO model results. These findings confirm the good performance of HY-2A RA for retrieving semidiurnal tides in the global ocean.

Key words: HY-2A satellite, radar altimeter, ocean tide, tide analysis

Citation: Yang Jungang, Jia Yongjun, Fan Chenqing, Cui Wei. 2023. Preliminary results of the global ocean tide derived from HY-2A radar altimeter data. Acta Oceanologica Sinica, 42(2): 65–73, doi: 10.1007/s13131-022-2025-1

1 Introduction

An ocean tide refers to the periodic vertical fluctuation and horizontal reciprocating movement of sea water under the action of celestial body tidal forces, such as the moon and the sun. Tides are an important factor affecting sea surface fluctuations and variations in ocean circulation and have an important impact on the variations in Earth's rotation and the restoration of satellite gravity fields. People began to study ocean tides very early, and ocean tide studies have gone through several developmental stages. In 1687, Newton proposed the equilibrium tide theory based on statics, marking the beginning of modern tide research. In 1776, Laplace organically combined tidal statics and dynamics to establish the Laplace tidal equations. In 1883, Darwin (2009) proposed a harmonic tidal analysis method. Doodson (1921) quoted a more precise lunar motion formula to further derive the harmonic expansion of tides. Munk and Cartwright (1966) proposed a tidal response analysis method based on the idea of signals and systems. In 1975, Groves et al. corrected the response function and proposed the orthogonal response method (Zhang et al., 2015). In 1980, the first global ocean tide model was constructed (Schwiderski, 1980). Inspired by the needs of navigation and restricted by *in situ* observations, the knowledge of ocean tides remained confined to the vicinity of coastlines and midocean islands where tides can be directly observed. Although global ocean tide studies are attractive, challenges must be faced when conducting this research due to the lack of observational data. At the same time, global ocean tide research critically influences the study and application of many fields, especially geodesy, geophysics and astronomy (Lambeck, 1977).

Determining accurate cotidal charts is the key to global ocean tide research. Historically, tides were measured only by tide gauges along continental coastlines or by bottom-pressure recorders located at a few hundred deep-sea sites near islands. Since the advent of satellite altimetry in the late 1970s, tide studies have entered a new era called the "Altimetry Era". Altimeters can directly measure travel times, thus recording the distance from the satellite to the sea surface. After various range corrections, the sea surface height can be calculated relative to the reference ellipsoid. Therefore, each observation point on the satellite ground track can essentially be regarded as a tide gauge station in the ocean. The advent of satellite altimetry has been totally revolutionary: it offers, for the first time, a means to estimate tides everywhere over the global oceans. The Geosat satellite launched in 1985 provided the first altimetric data for global tide research, and a global ocean tide model with an improved accuracy over the Schwiderski model was derived (Cartwright and Ray, 1991). Le Provost (2001) identified four main approaches for the development of tidal models using satellite altimeter data. These approaches include the direct empirical tidal analysis of altimetry; the empirical tidal analysis of altimeter residuals after first removing a prediction derived with an adopted prior model; the tidal analysis of altimetry in terms of some kind of spatial basis

Foundation item: The National Key Research and Development Program of China under contract No. 2016YFC1401801.
*Corresponding author, E-mail: jiayongjun@mail.nsoas.org.cn

functions; and the use of inverse methods that solve the hydrodynamic equations via data-assimilation techniques. The direct empirical tidal analysis altimetry methods mainly include two kinds: harmonic analysis methods (Doodson, 1921, 1958) and orthotide formulation methods (Munk and Cartwright, 1966). Since the launch of TOPEX/POSEIDON (T/P) and its successors (Jason-1/2/3 and other altimetry missions), studies on global ocean tides have progressed dramatically with the development of models with unprecedented accuracies by many authors. These latest global ocean tide model versions include GOT4.8 (Ray, 1999), NAO.99 (Matsumoto et al., 2000), OSU12 (Fok, 2012), DTU10 (Cheng and Andersen, 2011), EOT20 (Hart-Davis et al., 2021), HAM12 (Taguchi et al., 2014), FES2014 (Carrere et al., 2016) and TPXO9 (Egbert and Erofeeva, 2002). These various models have been compared and evaluated against different global ocean tide models (Shum et al., 1997; Stammer et al., 2014).

The first Chinese ocean dynamic environmental satellite, HY-2A, was launched on August 16, 2011; this satellite first flew on a 14-day repeat polar sun-synchronous orbit with a mean altitude of 971 km. Since March of 2016, the HY-2A satellite course changed to a 168-day repeat orbit with a mean altitude of 973 km to complete the geodetic mission. A dual-frequency radar altimeter (Ku-band and C-band), which was designed to measure the sea surface height (SSH), sea surface wind speed, and significant wave height, was equipped on the HY-2A (Jiang et al., 2012). The HY-2A satellite stopped working in June of 2020. HY-2B, HY-2C and HY-2D, the successors of HY-2A, are also equipped radar altimeters and were launched on October 25, 2018, September 21, 2020 and May 19, 2021, respectively. With the 14-day repeat-orbit HY-2A SSH data covering a period more than 2.5 years, the global ocean tides can be retrieved by the HY-2 altimeter.

In this paper, the preliminary global ocean tide results retrieved by the HY-2A radar altimeter are presented with the tide harmonic analysis method, and the results are compared to tidal gauge data and the results of the TPXO tide model. The second section provides a brief overview of the HY-2A data, tidal gauge data, TPXO model and harmonic analysis method. In the third section, global ocean tides are retrieved from the HY-2A altimeter data. The fourth section analyzes the retrieved global ocean tide results by comparing the results to tidal gauge data and the TPXO model results. Finally, the main results of this paper are concluded in the fifth section.

2 Data and methods

2.1 *HY-2A radar altimeter data*

The HY-2A satellite, which is equipped a radar altimeter (RA), was the first Chinese oceanic dynamic environment monitoring satellite. The HY-2A RA has a repeat cycle of 14 days, and there are 386 passes in a single HY-2A cycle. The along-track spatial resolution is approximately 7 km. The maximum distance between two adjacent tracks at the equator is close to 200 km. The latitude coverage is between 80°S and 80°N. Limited by the display effect, it is impossible to clearly show all the ground orbits of the HY-2A RA in one map. The ground tracks in the northern Pacific Ocean are shown in Fig. 1. Time-series SSH data can be obtained at the same measuring points from the long-period HY-2A RA data. The level-2 GDR data of the HY-2A RA during the period spanning from November 1, 2011 to August 16, 2014 (75 cycles), distributed by the National Satellite Ocean Application Service (NSOAS), are used in this study. The altitude of the satellite, the range between the satellite and sea surface, all range corrections, including the dry and wet tropospheric corrections, ionospheric corrections, sea state bias corrections and other geophysical corrections, are involved in the GDR data of HY-2A RA, and the SSH can be calculated using these parameters.

2.2 *Tidal gauge data*

To validate the tidal harmonic constants of the different tidal constituents retrieved by the HY-2A RA data, tidal constants from the Permanent Service for Mean Sea Level and World Ocean Circulation Experiment (WOCE) are collected in this study. Pelagic tidal constants (for tidal constituents Q_1, O_1, P_1, K_1, N_2, M_2, S_2, and K_2) are derived from sea bed pressure recorders located remotely from land (Smithson, 1992). Tidal harmonic constants (the amplitude and phase lag of each tidal constituent), which were produced by analyzing the full multiyear time series recorded at each station, are derived from the WOCE "delayed-mode" sea level Data Assembly Centre operated by BODC and used in this study. In addition, the tidal constants in the Chinese coastal area are also used (Fang et al., 2004; Zu et al., 2008). A total of 119 stations are considered, and the spatial distribution of these tidal gauge data is shown in Fig. 2.

2.3 *TPXO tide model*

TPXO9 is the latest version of a series of tidal solutions (elevations plus barotropic currents) produced using a representer-

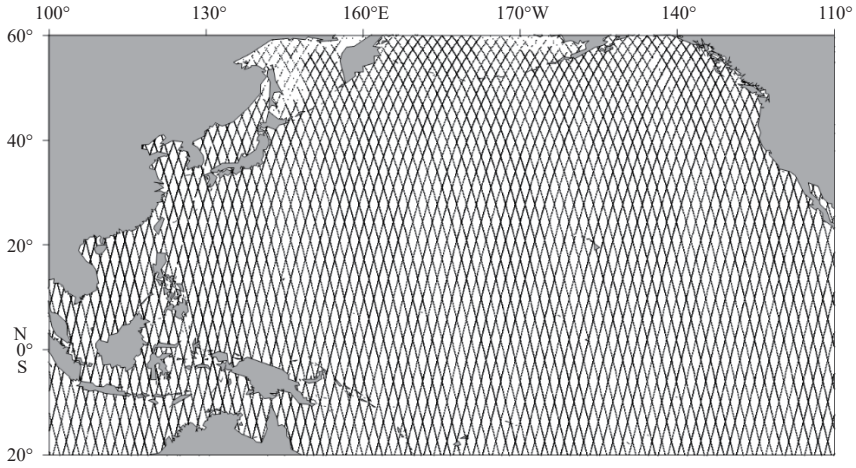

Fig. 1. Sketch map of the ground tracks of the HY-2A RA in the northern Pacific Ocean. The black lines show the ground tracks of the HY-2A RA.

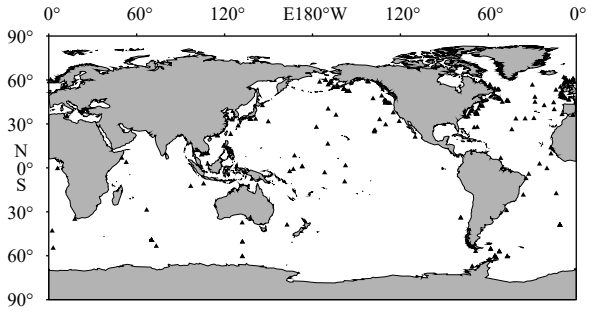

Fig. 2. Spatial distribution of the tidal constant data used in the study. The triangles indicate the locations of the tidal gauges.

based variational scheme to assimilate satellite altimetry data, and sometimes other data, into a global shallow-water model (Egbert and Erofeeva, 2002). Fifteen tidal constituents named M_2, S_2, N_2, K_2, K_1, O_1, P_1, Q_1, Mm, Mf, M_4, Mn_4, MS_4, $2n_2$ and S_1 are included in the TPXO atlas. TPXO9 has a resolution of (1/6)°. Compared to other tidal models, the TPXO9 model has the best precision and spatial resolution in the global ocean, so the tidal constants of the TPXO9 model are used herein to validate the global ocean tides retrieved from the HY-2A RA data.

2.4 *Tidal harmonic analysis method*

According to equilibrium tide theory, a tide can be regarded as the superposition of many tidal constituents with different cycles. In this study, eight tidal constituents (M_2, S_2, N_2, K_2, K_1, O_1, P_1, and Q_1) are considered. The harmonic analysis expression of the tide height at any point on the satellite orbit can be described as follows (Doodson, 1958; Fang et al., 1986, 2004):

$$h(t) = H_0 + \sum_{i=1}^{8} f_i H_i \cos[\omega_i t + (V_{0i} + u_i) - g_i], \tag{1}$$

where h is SSH relative to mean sea surface obtained by the altimeter, t is the altimeter measuring time, H_0 is the mean sea surface, H is the amplitude of the tidal constituent, g is the phase lag of the tidal constituent, ω is the angular speed, f is the nodal factor, and $V_0 + u$ is the initial phase of the equilibrium tide, with u representing the nodal adjustment angle of the initial phase. The initial phase and angular speed are listed in Table 1. The nodal factor f and nodal adjustment angle u for different tidal constituents are given in Appendix.

s, h_1, p, N and p_1 used in Table 1 and Appendix are basic astronomical elements that can be obtained using the following expressions.

$$\begin{cases} s = 277.02 + 129.384\,8\,(y-1900) + 13.176\,4\left(D + Y + \dfrac{t}{24}\right) \\ h_1 = 280.19 - 0.238\,7\,(y-1900) + 0.985\,7\left(D + Y + \dfrac{t}{24}\right) \\ p = 334.39 + 40.662\,5(y-1900) + 0.111\,4\left(D + Y + \dfrac{t}{24}\right) \\ N = 259.157 - 19.328\,2(y-1900) - 0.053\,0\left(D + Y + \dfrac{t}{24}\right) \\ p_1 = 281.22 + 0.017\,2(y-1900) + 0.000\,05\left(D + Y + \dfrac{t}{24}\right), \end{cases} \tag{2}$$

where y is the year of measurement, D is the number of days from 1 January of year y (where 1 January is the 0th day), Y is the number of leap years from 1900 to year y, and t is the hour.

Table 1. Initial phase and angular speed of the tidal constituents

Tidal constituent	V_0 /(°)	ω/((°)·h^{-1})
M_2	$360-2s+2h_1$	28.984 104 24
S_2	360	30.000 000 00
K_2	$360+2h_1$	30.082 137 28
N_2	$360-3s+2h_1+p$	28.439 729 54
K_1	$90+h_1$	15.041 068 64
O_1	$270-2s+h_1$	13.943 035 59
P_1	$270-h_1$	14.958 931 36
Q_1	$270-3s+h_1+p$	13.398 660 88

Expression (1) can be expanded to the following equation:

$$\begin{aligned} h(t) =& H_0 + \sum_{i=1}^{8}\{H_i f_i \cos g_i \cos[\omega_i t + (V_{0i} + u_i)] + \\ & H_i f_i \sin g_i \sin[\omega_i t + (V_{0i} + u_i)]\}, \end{aligned} \tag{3}$$

$$h(t) = H_0 + \sum_{i=1}^{8}\{A_i f_i \cos[\omega_i t + (V_{0i} + u_i)] + B_i f_i \sin[\omega_i t + (V_{0i} + u_i)]\}, \tag{4}$$

where $A_i = H_i \cos g_i$ and $B_i = H_i \sin g_i$.

With the time series data representing altimeter-measured SSHs, parameters A and B can be resolved by the least square method. Then, the constants of the tidal constituents can be obtained by determining A and B.

3 Tidal analysis

Performing a global ocean tide analysis using HY-2A RA data mainly involves three steps. First, the HY-2 RA data are preprocessed, and the SSH relative to the mean sea surface (that is, the sea level anomaly or SLA) is obtained at each point on the ground track. Second, to determine the reference cycle of HY-2A RA and to collinearly process all cycle data to the time series data of each point on the ground track of the reference cycle, a 3σ-standard is used to eliminate outliers in the time series data. Finally, tidal constants are obtained by the HY-2A RA time series data using the least square method. The technical flow of the process by which global ocean tide analysis is performed using HY-2A RA data is shown in Fig. 3.

3.1 *HY-2A RA data processing*

A satellite altimeter directly measures the distance from the satellite to the instantaneous sea surface. Because the traveling of electromagnetic waves is affected by physical factors such as the atmosphere during their propagation process, it is necessary to perform dry and wet tropospheric corrections, an ionospheric correction, a sea state bias correction, an inverted barometer correction and a high-frequency fluctuation correction to calculate the SSH. In addition, the mean sea surface (MSS), solid earth tide (SET), pole tide (PT) and load tide (LT) are removed from the SSH to obtain the sea surface height information (also called the sea surface height anomaly or SLA), which is used in the subsequent tidal analysis considering altimeter data. The expression used to calculate the SLA is given as follows:

$$\begin{aligned} h =& \mathrm{SSH} - \mathrm{MSS} - \mathrm{SET} - \mathrm{PT} - \mathrm{LT} = H_{\mathrm{alt}} - (R + R_{\mathrm{d}} + \\ & R_{\mathrm{w}} + R_{\mathrm{i}} + R_{\mathrm{SSB}} + \mathrm{IB} + \mathrm{HF}) - \mathrm{MSS} - \mathrm{SET} - \mathrm{PT} - \mathrm{LT}, \end{aligned} \tag{5}$$

where H_{alt} is the altitude of the satellite, R is the range measured

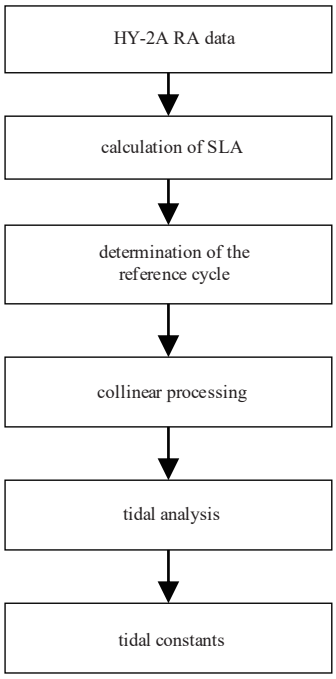

Fig. 3. Technical flow of the tidal analysis process using HY-2A RA data.

by the altimeter, R_d is the dry tropospheric correction, R_w is the wet tropospheric correction, R_i is the ionospheric correction, R_{SSB} is the sea state bias correction, IB is the inverted barometer correction and HF is the high-frequency fluctuation correction. The MSS is obtained from the CNES_CLS2015 model (Pujol et al., 2018).

According to the data quality control standards (data editing criteria) provided in the HY-2A RA user manual, the SLA data of all HY-2A RA cycles are calculated using the level-2 GDR data provided by NSOAS. Considering that the tide heights are less than 5 m in most areas of the global ocean, any HY-2A RA SLAs larger than 5 m are removed. The repetition period of the HY-2A RA is 14 days. In theory, this means that the ground tracks repeat exactly every 14 days and that the measurement of every point on the ground track is repeated exactly every 14 days. However, the ground tracks of different cycles exhibit little differences due to orbital drift. To obtain the SLA time series on the same measuring point of the ground track, the reference cycle must first be determined by comparing the different HY-2A RA cycles. The HY-2A RA cycle with the most observation data is regarded as the reference cycle. More than 220 000 measuring points are contained in each reference cycle. Then, the HY-2A RA data of different cycles are processed using the measuring points of the reference cycle by bilinear interpolation. Finally, the time-series SLA data at all measuring points of the reference cycle are obtained. Figure 4 is an example of these time-series SLA data.

3.2 *Tidal constants retrieved by the HY-2A RA*

Because the ocean tide sampling frequency by HY-2A RA (1/(14×24) cph, cph: cycleperhour) is largely less than the diurnal tide (approximately 1/24 cph) and semidiurnal tide (approximately 1/12 cph) frequencies, the tide aliasing effect must be considered when analyzing altimeter data (Schlax and Chelton, 1994). At each measuring point on the ground track, the sea surface heights are sampled at a time interval equal to the orbital repeat period of the satellite. The Nyquist critical frequency corresponding to the sampling interval is calculated as follows:

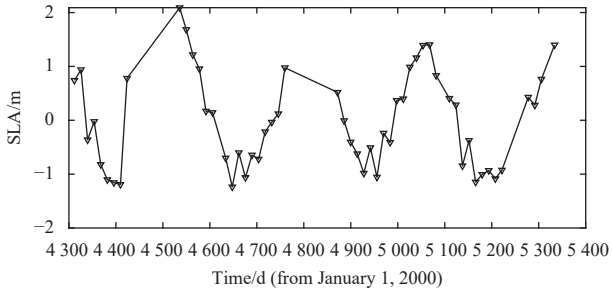

Fig. 4. Time series sea level anomaly (SLA) data obtained at one HY-2A RA measurement point.

$$f_c = 1/(2\Delta t). \tag{6}$$

A tidal constituent of frequency f may have a given number of alias frequencies calculated as follows (Godin, 1972):

$$f_a(m) = 2mf_c \pm f, \quad m = 0, 1, 2, \cdots \tag{7}$$

The particular alias frequency can be calculated using the following formula:

$$f_a = \min |2mf_c \pm f|, \quad m = 0, 1, 2, \cdots \tag{8}$$

The alias periods for each constituent are shown in Table 2. Because the HY-2A RA repeat period is an integer day, tidal constituent S_2 cannot be distinguished in the HY-2A RA data. The alias period of tidal constituent O_1 of 1 036.74 days is the largest and is close to the period of the HY-2A RA data. In general, the tidal constituents S_2 and O_1 cannot be retrieved from HY-2A RA data.

To fully resolve the two constituents of alias frequencies f_{a1} and f_{a2}, the measurement time span T must satisfy the Rayleigh criterion, that is, $T \geqslant 1/|f_{a1} - f_{a2}|$. The time span required for the phase difference between the two associated constituents to reach 1 cycle is called their alias synodic period (Fang et al., 2004). The HY-2A RA alias synodic periods of each pair of constituents are listed in Table 3.

Table 3 shows that tidal constituents K_1 and P_1 cannot be distinguished in the HY-2A RA data because their alias synodic period (653.36 years) is much greater than the period of the HY-2A RA data. In general, we conclude from the above alias period analysis that diurnal tides cannot be resolved in the HY-2A RA data. This is also confirmed by the tidal analysis results described in the next section.

With the time-series HY-2A RA SLA data recorded during the period lasting from 2011 to 2014, the global ocean tidal constants of different tidal constituents are retrieved by the least square method introduced in Section 2.4. The tidal constants of 8 tidal constituents (M_2, S_2, N_2, K_2, K_1, O_1, P_1, and Q_1) are calculated, but the results of the diurnal tidal constituents (K_1, O_1, P_1, and Q_1) are

Table 2. Tidal periods and alias periods of the HY-2A RA

	M_2	S_2	K_2	N_2	K_1	O_1	P_1	Q_1
Tidal period/d	0.517 53	0.5	0.498 63	0.527 43	0.997 27	1.075 81	0.498 63	0.527 43
Alias period/d	270.13	infinity	182.62	30.68	365.23	1 036.74	365.79	28.31

aliased together and cannot be distinguished, and tidal constituent S_2 is aliased into the mean sea surface because the tidal height of S_2 remains the same over the time interval of 14 days. Therefore, only tidal constituents M_2, N_2, and K_2 are retrieved precisely from the HY-2A RA data.

Table 3. HY-2A alias synodic periods of each pair of constituents (years)

	M_2	S_2	K_2	N_2	K_1	O_1	P_1	Q_1
M_2	–	0.74	1.54	0.09	2.84	1.00	2.83	0.09
S_2	0.74	–	0.50	0.08	1.00	2.84	1.00	0.08
K_2	1.54	0.50	–	0.10	0.09	0.61	1.00	0.09
N_2	0.09	0.08	0.10	–	0.09	0.09	0.09	1.00
K_1	2.84	1.00	1.00		–	1.54	653.36	0.08
O_1	1.00	2.84	0.61	0.09	1.54	–	1.55	0.08
P_1	2.83	1.00	1.00	0.09	653.36	1.55	–	0.08
Q_1	0.09	0.08	0.09	1.00	0.08	0.08	0.08	–

Note: – represents no data.

4 Results and discussion

4.1 *Comparison with tidal gauge data*

To evaluate the tidal analysis results obtained from the HY-2A RA data, the tidal constants retrieved by the HY-2A RA are compared to those obtained from the tidal gauge data introduced in Section 2.2. The data matching criteria is the spatial distance between the HY-2A RA observation point and tidal gauge is less than 10 km. The comparisons of tidal constituents M_2, N_2 and K_2

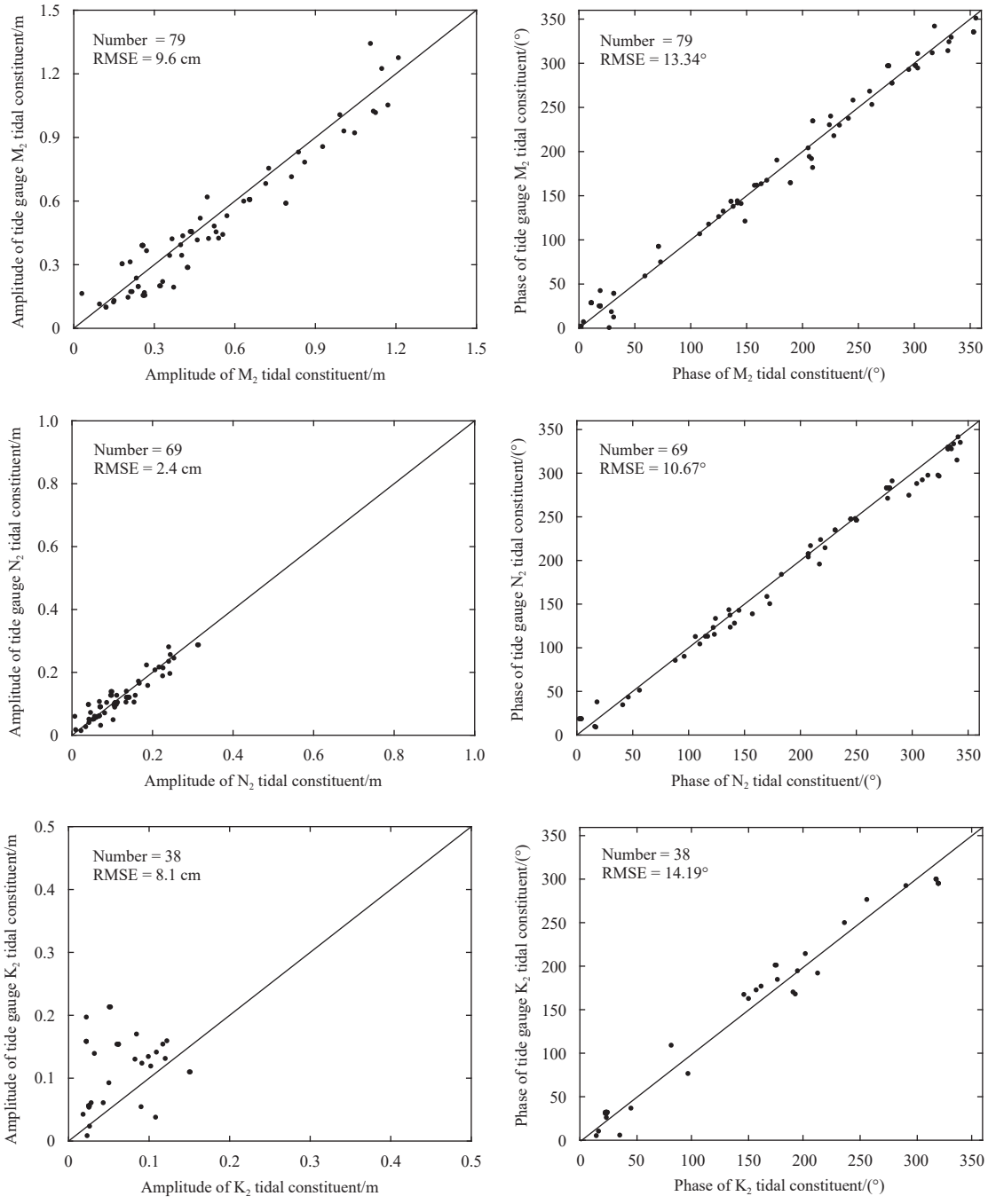

Fig. 5. Comparisons of the tidal constants of the tidal constituents M_2, N_2 and K_2 between the retrieved results and tidal gauge data.

are shown in Fig. 5. The numbers of matching points are 79, 69 and 38 for tidal constituents M_2, N_2 and K_2, respectively. The amplitudes and phases of the tidal constituents have good consistency with the tidal gauge data except the amplitude of tidal constituent K_2, which is mainly below 0.2 m. The biases and root mean square errors (RMSEs) of the amplitude and phase lag values are calculated between the HY-2A results and tidal gauge data. The RMSEs of the amplitude and phase lag are 9.6 cm and 13.34°, 2.4 cm and 10.47°, and 8.1 cm and 14.19° for tidal constituents M_2, N_2, and K_2, respectively. These results indicate that the M_2, N_2 and K_2 tidal constants retrieved by the HY-2A RA have good precision, confirming the good performance of the HY-2A RA for retrieving semidiurnal global ocean tides. The analysis of the RMSEs of diurnal tides confirms that they cannot be distinguished or retrieved from the HY-2A RA data in the considered data period.

4.2 *Comparison with the TPXO tide model*

Considering the sparse spatial distribution of the tidal gauge data, the tidal analysis results are also compared with the TPXO model results in addition to being compared with the tidal gauge data. The comparisons of tidal constituents M_2 and N_2 are shown in Fig. 6. The tidal constituent M_2 exhibits good consistency between the tidal analysis results and the TPXO model. There is a

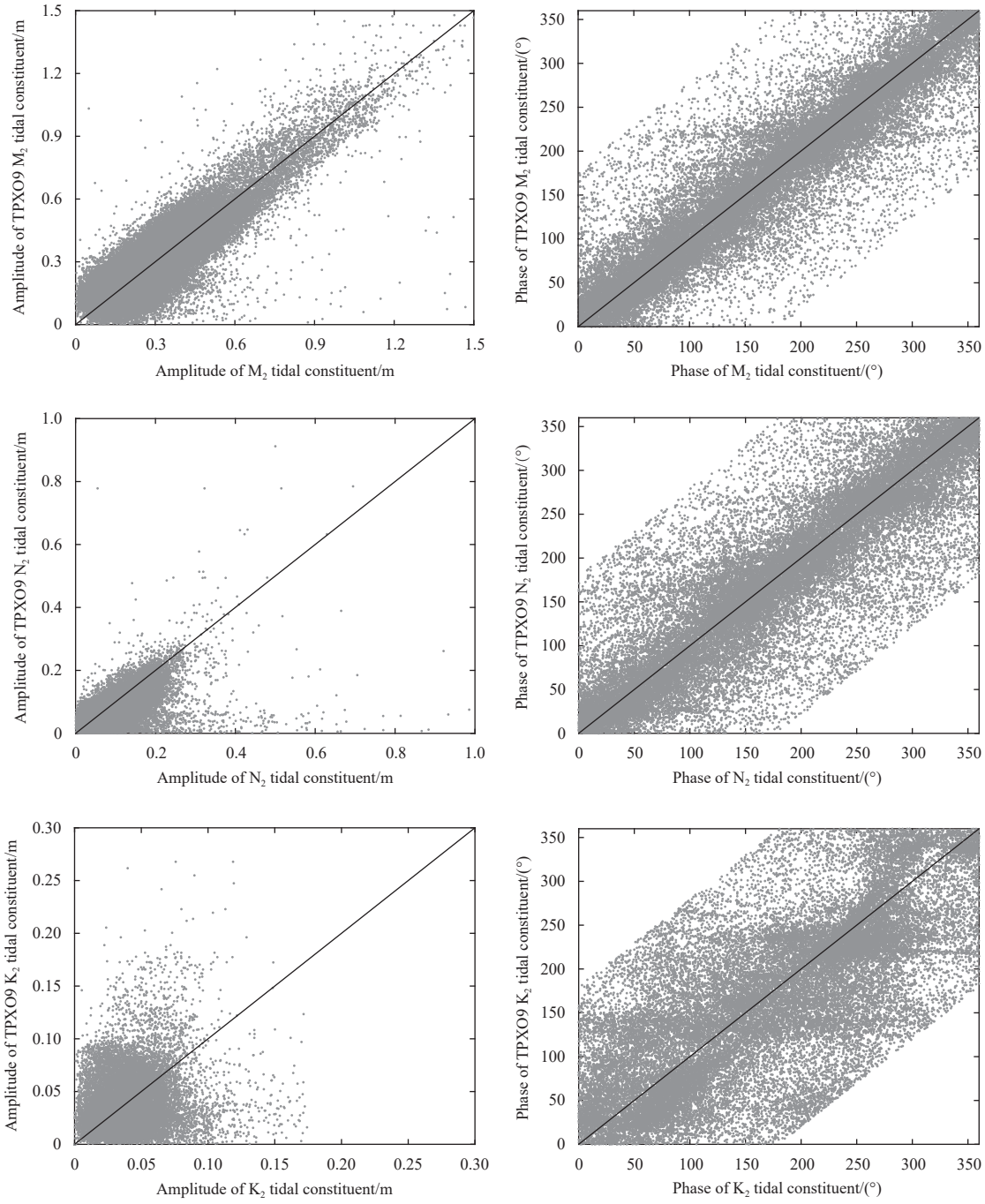

Fig. 6. Comparisons of the tidal constants of the tidal constituents M_2, N_2 and K_2 between the retrieved results and the TPXO model results.

large deviation regarding the amplitude of tidal constituent N_2 when the amplitude is below 0.1 m. The largest differences in tidal constants are located near coasts or islands. These results also confirm the good performance of the HY-2A RA in retrieving the semidiurnal tides of the global ocean. The RMSEs of the tidal constants between the retrieved results and the TPXO model also confirm the good performance of the HY-2A RA.

The retrieved tidal constants of tidal constituent M_2 are distributed irregularly along the ground track of the HY-2A satellite. To conveniently analyze the distribution of these tidal constants, the retrieved tidal constants of tidal constituent M_2 are gridded by the Kriging method (Oliver and Webster, 1990). Along with the gridded tidal constants of the retrieved tidal constituent M_2, the M_2 cotidal chart is shown in Fig. 7. The M_2 cotidal chart of the TPXO model is also shown in Fig. 7. It can be seen in Fig. 7 that the M_2 cotidal charts of the retrieved results and TPXO model results are very consistent. The number of amphidromic points of the M_2 tidal constituent retrieved from the HY-2A RA data is completely consistent with that of the TPXO model, and the locations of amphidromic points are basically the same. The spatial distribution of the M_2 amplitude is also consistent with the TPXO model. The contour of the M_2 phase lag is not as smooth as the TPXO model result, and this finding is consistent with the small phase lag fluctuations in the real ocean due to the existence of internal tides. The M_2 phase lag data are subjected to spatial low-pass filtering to smooth the isoline, as shown in Fig. 7. In general, the M_2 tidal constituent information can be accurately extracted from the HY-2A RA data. This finding also supports the ability of the HY-2A altimeter to extract global-ocean M_2 tides.

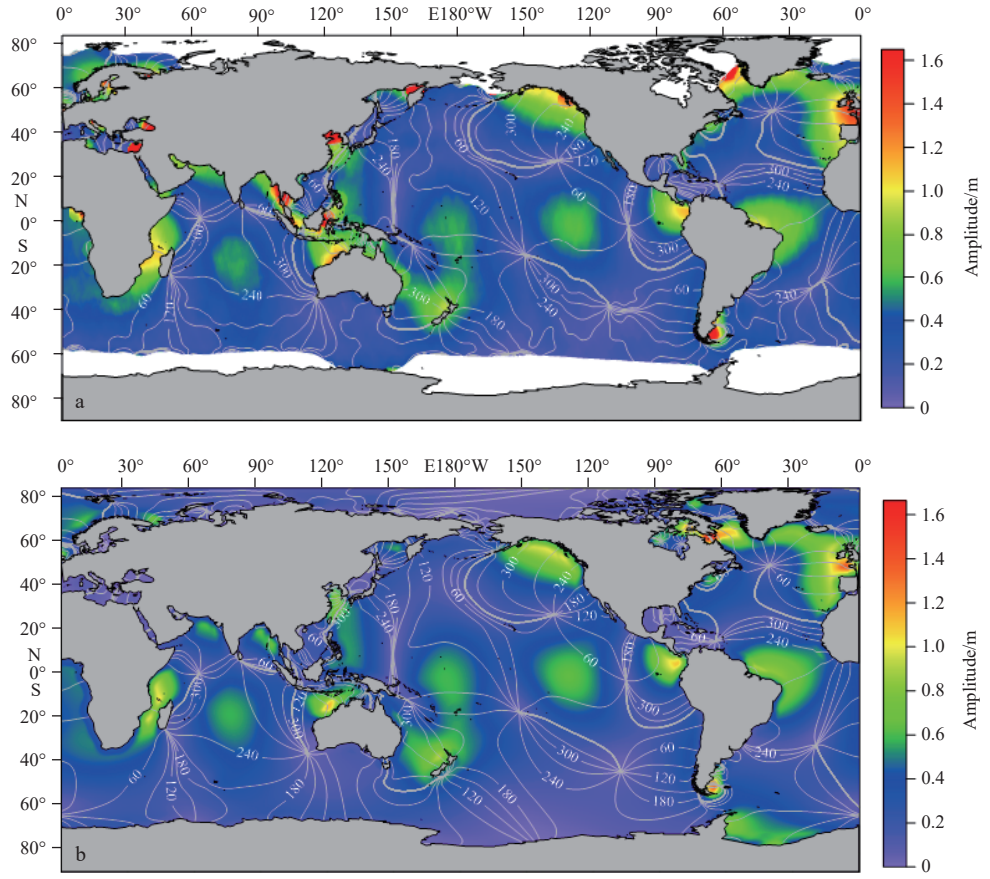

Fig. 7. Comparison of the M_2 cotidal chart between the tidal constants retrieved by the HY-2A RA (a) and the TPXO model (b). The lines show the phase lag distributions (in (°)), and the colors show the amplitudes.

5 Conclusions

The first Chinese ocean dynamic environmental satellite, HY-2A, was launched on August 16, 2011 and was equipped with a radar altimeter; this satellite first flew on a 14-day repeat polar sun-synchronous orbit. The HY-2A RA data recorded from November 1, 2011 to August 16, 2014 are used herein to extract global ocean tides. The tidal constants of 8 tidal constituents are extracted from the HY-2A RA data with harmonic analysis based on the least square method. Considering tide-aliasing issues, the analyses of the alias periods and alias synodic periods of different tidal constituents show that the diurnal and semidiurnal tides of S_2 cannot be extracted from the HY-2A RA data. This is caused by the repeat period and the period of the HY-2A RA data used in this study. Therefore, only tidal constituents M_2, N_2, and K_2 are retrieved precisely from the HY-2A RA data. The tidal constants of tidal constituents M_2, N_2 and K_2 are compared to those obtained from tidal gauge data and the TPXO tide model. Compared to the tidal gauge data, the RMSEs of amplitude and phase lag are less than 0.1 m and 15°, respectively. The comparisons of the semidiurnal tides with the TPXO model results show that these tidal constituents have good consistency with the TPXO model results. These results confirm the good performance of the HY-2A RA in retrieving the semidiurnal tides of the global ocean. With the successful launch of HY-2B, HY-2C and HY-2D on October 25, 2018, September 21, 2020 and May 19, 2021 and with the long-time-series data accumulation of these HY-2-series alti-

meters, global ocean tides will be retrievable by these HY-2 series altimeters in more detail in the future.

Acknowledgements

The authors would like to thank the National Satellite Ocean Application Service, Beijing, China for providing HY-2A RA data; Permanent Service for Mean Sea Level, for providing tide gauge data; National Oceanography Centre British Oceanographic Data Centre, for providing tidal constants data from the WOCE "delayed-mode" sea level Data Assembly Centre; and Egbert & Erofeeva, CEOAS, Oregon State University for providing the TPXO tide model.

References

Carrere L, Lyard F, Cancet M, et al. 2016. FES 2014: a new tidal model-Validation results and perspectives for improvements. Prague: ESA Living Planet Conference

Cartwright D E, Ray R D. 1991. Energetics of global ocean tides from Geosat altimetry. Journal of Geophysical Research: Oceans, 96(C9): 16897–16912, doi: 10.1029/91JC01059

Cheng Yongcun, Andersen O B. 2011. Multimission empirical ocean tide modeling for shallow waters and polar seas. Journal of Geophysical Research: Oceans, 116(C11): C11001, doi: 10.1029/2011JC007172

Darwin G. 2009. The harmonic analysis of tidal observations. In: The Scientific Papers of Sir George Darwin: Oceanic Tides and Lunar Disturbance of Gravity (Cambridge Library Collection-Physical Sciences). Cambridge: Cambridge University Press, 1–69, doi: 10.1017/CBO9780511703461

Doodson A T. 1921. The harmonic development of the tide-generating potential. Proceedings of the Royal Society A: Mathematical, Phyaical and Engineering Sceinces, 100(704): 305–329

Doodson A T. 1958. Oceanic tides. Advances in Geophysics, 5: 117–152

Egbert G D, Erofeeva S Y. 2002. Efficient inverse modeling of barotropic ocean tides. Journal of Atmospheric and Oceanic Technology, 19(2): 183–204, doi: 10.1175/1520-0426(2002)019<0183:EIMOBO>2.0.CO;2

Fang Guohong, Wang Yonggang, Wei Zexun, et al. 2004. Empirical cotidal charts of the Bohai, Yellow, and East China Seas from 10 years of TOPEX/Poseidon altimetry. Journal of Geophysical Research: Oceans, 109(C11): C11006, doi: 10.1029/2004JC002484

Fang Guohong, Zheng Wenzhen, Chen Zongyong, et al. 1986. Analysis and Prediction of Tides and Tidal Currents (in Chinese). Beijing: China Ocean Press

Fok H S. 2012. Ocean Tides Modeling Using Satellite Altimetry. Columbus: Ohio State University

Godin G. 1972. The Analysis of Tides. Toronto: University of Toronto Press

Hart-Davis M G, Piccioni G, Dettmering D, et al. 2021. EOT20: A global ocean tide model from multi-mission satellite altimetry. Earth System Science Data, 13(8): 3869–3884, doi: 10.5194/essd-13-3869-2021

Jiang Xingwei, Lin Mingsen, Liu Jianqiang, et al. 2012. The HY-2 satellite and its preliminary assessment. International Journal of Digital Earth, 5(3): 266–281, doi: 10.1080/17538947.2012.658685

Lambeck K. 1977. Tidal dissipation in the oceans: Astronomical, geophysical and oceanographic consequences. Philosophical Transactions of the Royal Society of London. Series A, Mathematical and Physical Sciences, 287(1347): 545–594, doi: 10.1098/rsta.1977.0159

Le Provost C. 2001. Ocean tides. In: Fu L L, Cazenave A, eds. Satellite Altimetry and Earth Sciences: A Handbook of Techniques and Applications. San Diego, CA: Academic Press, 69: 267–303

Matsumoto K, Takanezawa T, Ooe M. 2000. Ocean tide models developed by assimilating TOPEX/POSEIDON altimeter data into hydrodynamical model: A global model and a regional model around Japan. Journal of Oceanography, 56(5): 567–581, doi: 10.1023/A:1011157212596

Munk W H, Cartwright D E. 1966. Tidal spectroscopy and prediction. Philosophical Transactions of the Royal Society A: Mathematical, Physical and Engineering Sciences, 259(1105): 533–581

Oliver M A, Webster R. 1990. Kriging: A method of interpolation for geographical information systems. International Journal of Geographical Information Systems, 4(3): 313–332, doi: 10.1080/02693799008941549

Pujol M I, Schaeffer P, Faugère Y, et al. 2018. Gauging the improvement of recent mean sea surface models: A new approach for identifying and quantifying their errors. Journal of Geophysical Research: Oceans, 123(8): 5889–5911, doi: 10.1029/2017JC013503

Ray R D. 1999. A global ocean tide model from Topex/Poseidon altimetry: GOT99.2. Greenbelt, MD: Goddard Space Flight Center

Schlax M G, Chelton D B. 1994. Aliased tidal errors in TOPEX/Poseidon sea surface height data. Journal of Geophysical Research: Oceans, 99(C12): 24761–24775, doi: 10.1029/94JC01925

Schwiderski E W. 1980. On charting global ocean tides. Reviews of Geophysics, 18(1): 243–268, doi: 10.1029/RG018i001p00243

Shum C K, Woodworth P L, Andersen O B, et al. 1997. Accuracy assessment of recent ocean tide models. Journal of Geophysical Research: Oceans, 102(C11): 25173–25194, doi: 10.1029/97JC00445

Smithson M J. 1992. Pelagic tidal constants-3. IAPSO Publication Scientifique No. 35. Trieste: The International Association for the Physical Sciences of the Ocean (IAPSO) of the International Union of Geodesy and Geophysics, 191

Stammer D, Ray R D, Andersen O B, et al. 2014. Accuracy assessment of global barotropic ocean tide models. Reviews of Geophysics, 52(3): 243–282, doi: 10.1002/2014RG000450

Taguchi E, Stammer D, Zahel W. 2014. Inferring deep ocean tidal energy dissipation from the global high-resolution data-assimilative HAMTIDE model. Journal of Geophysical Research: Oceans, 119(7): 4573–4592, doi: 10.1002/2013JC009766

Zhang Shenghai, Lei Jintao, Li Fei. 2015. Advances in global ocean tide models. Advances in Earth Science (in Chinese), 30(5): 579–588, doi: 10.11867/j.issn.1001-8166.2015.05.0579

Zu Tingting, Gan Jianping, Erofeeva S Y. 2008. Numerical study of the tide and tidal dynamics in the South China Sea. Deep-Sea Research Part I: Oceanographic Research Papers, 55(2): 137–154, doi: 10.1016/j.dsr.2007.10.007

Appendix: Expression of *f* and *u* for different tidal constituents

With the Ep. (2) of s, h_1, p, N and p_1, the nodal factor f and nodal adjustment angle u for different tidal constituents are given in the following (Doodson, 1958; Fang et al., 1986, 2004).

Tidal constituent M_2,

$$\begin{cases} f_{M_2}\cos(u_{M_2}) = 1 + 0.000\,52\cos(2N) - 0.037\,33\cos(N) + 0.000\,58\cos(2p) + 0.000\,21\cos(2p - N) \\ f_{M_2}\sin(u_{M_2}) = 0.000\,52\sin(2N) - 0.037\,33\sin(N) + 0.000\,58\sin(2p) + 0.000\,21\sin(2p - N) \end{cases}. \tag{A1}$$

Tidal constituent S_2,

$$\begin{cases} f_{S_2}\cos(u_{S_2}) = 1 + 0.002\,25\cos(N) + 0.000\,14\cos(2p) \\ f_{S_2}\sin(u_{S_2}) = 0.002\,25\sin(N) + 0.000\,14\sin(2p) \end{cases}. \tag{A2}$$

Tidal constituent K_2,

$$\begin{cases} f_{K_2}\cos(u_{K_2}) = 1 + 0.285\,18\cos(N) + 0.032\,35\cos(2N) \\ f_{K_2}\sin(u_{K_2}) = -0.310\,74\sin(N) - 0.032\,35\sin(2N) \end{cases}. \tag{A3}$$

Tidal constituent N_2,

$$\begin{cases} f_{N_2}\cos(u_{N_2}) = 1 + 0.000\,52\cos(2N) - 0.037\,33\cos(N) + 0.000\,81\cos(p - p_1) - 0.003\,85\cos(2p - 2N) \\ f_{N_2}\sin(u_{N_2}) = 0.000\,52\sin(2N) - 0.037\,33\sin(N) + 0.000\,81\sin(p - p_1) + 0.003\,85\sin(2p - 2N) \end{cases}. \tag{A4}$$

Tidal constituent K_1,

$$\begin{cases} f_{K_1}\cos(u_{K_1}) = 1 + 0.000\,19\cos(2p - N) + 0.115\,73\cos(N) - 0.002\,81\cos(2N) \\ f_{K_1}\sin(u_{K_1}) = 0.000\,19\sin(2p - N) - 0.115\,39\sin(N) + 0.003\,03\sin(2N) \end{cases}. \tag{A5}$$

Tidal constituent O_1,

$$\begin{cases} f_{O_1}\cos(u_{O_1}) = 1 - 0.005\,78\cos(2N) + 0.188\,52\cos(N) - 0.001\,03\cos(2p - N) - 0.006\,45\cos(2p) + 0.000\,19\cos(2p + N) \\ f_{O_1}\sin(u_{O_1}) = -0.005\,78\sin(2N) + 0.188\,52\sin(N) - 0.001\,03\sin(2p - N) - 0.006\,45\sin(2p) + 0.000\,19\sin(2p + N) \end{cases}. \tag{A6}$$

Tidal constituent P_1,

$$\begin{cases} f_{P_1}\cos(u_{P_1}) = 1 + 0.000\,8\cos(2N) - 0.001\,5\cos(2p) - 0.011\,23\cos(N) - 0.000\,3\cos(2p - N) - 0.000\,4\cos(2p) \\ f_{P_1}\sin(u_{P_1}) = 0.000\,8\sin(2N) - 0.001\,5\sin(2p) - 0.011\,23\sin(N) - 0.000\,3\sin(2p - N) - 0.000\,4\sin(2p) \end{cases}. \tag{A7}$$

Tidal constituent Q_1,

$$\begin{cases} f_{Q_1}\cos(u_{Q_1}) = 1 + 0.188\,44\cos(N) - 0.005\,68\cos(2N) - 0.002\,77\cos(2p) - 0.003\,88\cos(2p - 2N) + \\ \qquad 0.000\,83\cos(p - p_1) - 0.000\,69\cos(2p - 3N) \\ f_{Q_1}\sin(u_{Q_1}) = 0.188\,44\sin(N) - 0.005\,68\sin(2N) - 0.002\,77\sin(2p) - 0.003\,88\sin(2p - 2N) + \\ \qquad 0.000\,83\sin(p - p_1) + 0.000\,69\sin(2p - 3N) \end{cases}. \tag{A8}$$